Science of the Total Environment 724 (2020) 138162

Contents lists available at ScienceDirect

Science of the Total Environment

journal homepage: www.elsevier.com/locate/scitotenv

Using large-scale climate drivers to forecast meteorological drought condition in growing season across the Australian wheatbelt

Puyu Feng [a,b], Bin Wang [b,*], Jing-Jia Luo [c], De Li Liu [b,d], Cathy Waters [e], Fei Ji [f], Hongyan Ruan [g], Dengpan Xiao [h], Lijie Shi [b,i], Qiang Yu [a,i,j,*]

[a] State Key Laboratory of Soil Erosion and Dryland Farming on the Loess Plateau, Northwest A&F University, Yangling 712100, Shaanxi, China
[b] NSW Department of Primary Industries, Wagga Wagga Agricultural Institute, Wagga Wagga, NSW 2650, Australia
[c] Institute for Climate and Application Research, Key Laboratory of Meteorological Disaster of Ministry of Education (KLME), Nanjing University of Information Science and Technology, Nanjing, China
[d] Climate Change Research Centre and ARC Centre of Excellence for Climate Extremes, University of New South Wales, Sydney, NSW 2052, Australia
[e] NSW Department of Primary Industries, Dubbo, NSW 2830, Australia
[f] Department of Planning, Industry and Environment, Queanbeyan, NSW 2620, Australia
[g] Guangxi Geographical Indication Crops Research Center of Big Data Mining and Experimental Engineering Technology, Key Laboratory of Beibu Gulf Environment Change and Resources Use Utilization of Ministry of Education, Nanning Normal University, Nanning 530001, China
[h] Institute of Geographical Sciences, Hebei Academy of Sciences, Shijiazhuang 050011, China
[i] School of Life Sciences, Faculty of Science, University of Technology Sydney, PO Box 123, Broadway, NSW 2007, Australia
[j] College of Resources and Environment, University of Chinese Academy of Science, Beijing 100049, China

HIGHLIGHTS

- A machine learning-based model was developed to predict drought.
- Lagged large-scale climate indices were adopted as input predictors.
- Growing season drought across all Australian cropping areas was predicted.
- Forecasted drought maps matched well with observed drought maps.
- NINO3.4 SST and MEI were identified as the most influential indices.

GRAPHICAL ABSTRACT

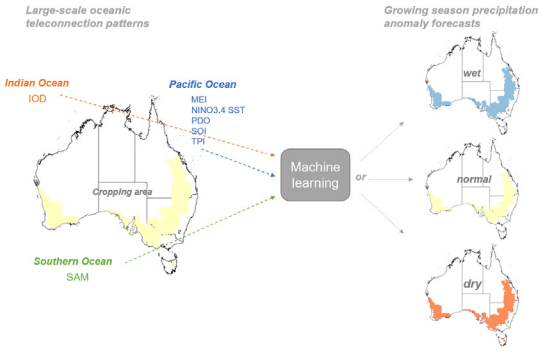

ARTICLE INFO

Article history:
Received 18 January 2020
Received in revised form 18 March 2020
Accepted 22 March 2020
Available online 27 March 2020

Editor: Jay Gan

Keywords:
Drought forecasting
Climate drivers

ABSTRACT

Recurring drought has caused large crop yield losses in Australia during past decades. Long-term drought forecasting is of great importance for the development of risk management strategies. Recently, large-scale climate drivers (e.g. El Niño-Southern Oscillation) have been demonstrated as useful in the application of drought forecasting. Machine learning-based models that use climate drivers as input are commonly adopted to provide drought forecasts as these models are easy to develop and require less information compared to physical-based models. However, few machine learning-based models have been developed to forecast drought conditions during growing season across all Australian cropping areas. In this study, we developed a growing season (Apr.-Nov.) meteorological drought forecasting model for each climate gauging location across the Australian wheatbelt based on multiple lagged (past) large-scale climate indices and the Random Forest (RF) algorithm. The Standardized Precipitation Index (SPI) was used as the response variable to measure the degree of

* Corresponding authors.
E-mail addresses: bin.a.wang@dpi.nsw.gov.au (B. Wang), yuq@nwafu.edu.cn (Q. Yu).

https://doi.org/10.1016/j.scitotenv.2020.138162

Random forest
Machine learning

meteorological drought. Results showed that the RF model could provide satisfactory drought forecasts in the eastern areas of the wheatbelt with Pearson's correlation coefficient $r > 0.5$ and normalized Root Mean Square Error ($nRMSE$) < 23%. Forecasted drought maps matched well with observed drought maps for three representative periods. We identified NINO3.4 sea surface temperature and Multivariate ENSO Index as the most influential indices dominating growing season drought conditions across the wheatbelt. In addition, lagged impacts of large-scale climate drivers on growing season drought conditions were long-lasting and the indices in previous year could also potentially affect drought conditions during current year. As large-scale climate indices are readily available and can be rapidly used to feed data driven models, we believe the proposed meteorological drought forecasting models can be easily extended to other regions to provide drought outlooks which can help mitigate adverse drought impacts.

1. Introduction

Australia is a major global wheat (mainly bread wheat and durum wheat) producer and exporter (GLNC, 2020). It produces 3% of the world's wheat production but accounts for nearly 15% of the world's annual global wheat trade (AEGIC, 2019). Thus, Australian wheat production is of central importance to ensure global wheat supply and food security. Wheat in Australia is mainly grown under rain-fed conditions, thus the wheat industry is sensitive to climate disasters, especially drought. Recurring drought events have resulted in large yield losses in the past decades. For example, the 2018 drought resulted in a 53% reduction in winter crop production in eastern Australia compared to the average of past 20 years (ABARES, 2019). Mitigating the impacts of drought on crop production has been a major research focus as early and reliable drought forecasting can assist farmers to undertake management decisions (e.g. sowing time) which will have financial implications. However, forecasting drought events remains a challenge to the scientific community because their triggers are complex and their features are variable in time and space.

Drought is a normal part of the climate in almost all regions of the world, which results from prolonged absence or shortage of rainfall in comparison with normal years (Zarch et al., 2015; Yu et al., 2020). Australia is the second driest continent on earth because it is located under the subtropical high-pressure belt, which prevents the lift of air required for rain (Williams and Stone, 2009). Australia is also a country prone to drought, as rainfall shows great inter-annual variability throughout the continent. It is well established that the variability of Australian rainfall is linked to the climatic anomalies originating from its surrounding oceans, including the Pacific, Indian, and Southern Oceans (Risbey et al., 2009). These climatic anomalies have been described by several dominant large-scale climate drivers. They include the Indian Ocean Dipole (IOD) which is expressed by the sea surface temperature (SST) gradient between the western and eastern tropical Indian Ocean (Saji and Yamagata, 2003), the El Niño Southern Oscillation (ENSO) defined by the SST anomalies in the central-eastern equatorial Pacific Ocean (McBride and Nicholls, 1983), the Southern Annular Mode (SAM) which refers to the atmospheric circulation in the mid- to high-latitudes of the southern hemisphere on interannual timescales (Marshall, 2003).

The teleconnections between large-scale climate drivers and Australia's rainfall conditions are among the strongest in the world (Kirono et al., 2010). Previous studies have suggested that Australia's extreme hydroclimatic events in the past two decades largely resulted from the anomalies of these climate drivers and their interactions (Xie et al., 2019). For example, the 2002–2009 'Millennium drought' was caused by a combination of long-term upward trend of SAM and prolonged lack of negative IOD phase (Ummenhofer et al., 2009). Following the Millennium drought, extreme wet periods (2010−2011) were found to be mostly driven by a sustained strong La Nina event (Luo et al., 2017), together with a concurrent positive SAM event (Gergis et al., 2012). The 2015 drought event originated from a strong El Niño event but was further enhanced by SAM and IOD variability (L'Heureux et al., 2017; Power and Delage, 2018). The drought events of recent decades in Australia occurred either across the entire continent or in specific regions, resulting in severe adverse impacts on crop production (Dijk et al., 2013). Thus, many studies have focused on empirical relationships between rainfall and large-scale climate drivers in order to provide timely and reliable climate outlooks and mitigate drought impacts (Risbey et al., 2009).

It is generally accepted that large-scale climate drivers have varying influences on rainfall in Australia which is dependent on geographic locations and seasons (Risbey et al., 2009). For example, the Nino 3.4 SST variability has been demonstrated to have a predominant impact on austral autumn rainfall in eastern Australia (van Rensch and Cai, 2014). SAM has been shown to mainly influence southern parts of Australia (Meneghini et al., 2007). Positive phases of SAM tend to result in an increase in spring rainfall in southwest Western Australia and New South Wales (King et al., 2014). There is generally, a negative correlation between IOD and rainfall from June to October in Western Australia, Victoria, South Australia, and southern New South Wales (Steptoe et al., 2018). It should also be noted that these relationships do not act independently, and each climate driver usually accounts for <20% of rainfall variability (Gallant et al., 2012; Risbey et al., 2009). Rainfall conditions throughout the Australian continent are generally the result of the synchronization of these climate drivers (Cleverly et al., 2016).

The teleconnections between large-scale climate drivers and Australian rainfall provide the scientific basis of data-driven drought forecast models (Abbot and Marohasy, 2014). Lagged values of large-scale climate drivers can be adopted as potential predictors of future drought conditions (Mera et al., 2018; Zhang et al., 2019). In the past few decades, a number of data-driven statistical models were developed within different regions of Australia for the forecasting of rainfall or drought conditions in the next month or season. For example, Mekanik et al. (2016) developed eight adaptive network-based fuzzy inference systems models based on lagged values of single or multiple climate drivers (ENSO, IOD, or Inter-decadal Pacific Oscillation) to forecast spring rainfall in Victoria. Their results suggested that the best performing models were able to forecast spring rainfall in a 10-year test period with acceptable correlation coefficients ($r = 0.29$–0.66) and low errors ($RMSE = 10.9$–25.0 mm) in 9 locations of Victoria. Abbot and Marohasy (2014) used artificial neural networks and lagged climate variables to forecast monthly rainfall with 1-month lead time in 3 sites of Queensland and achieved r values of >0.55. The two studies also demonstrated that statistical models developed using climate drivers performed better than the state-of-art dynamical model, the Predictive Ocean Atmosphere Model for Australia (POAMA) developed and run by the Australian Bureau of Meteorology. Physics-based dynamical weather forecasting models are normally considered as the mainstream approach by scientific community. However, dynamical models are usually expensive to operate and implement and rely overly on initial conditions. Despite of substantial technological advances and research efforts, dynamical models still have similar performance on seasonal rainfall forecasts in comparison to simple statistical models (Abbot and Marohasy, 2014). Thus, data-driven statistical models

based on large-scale climate drivers can still be used to provide seasonal rainfall forecasts effectively in various regions of Australia.

The Australian wheatbelt produces about 25 million tons wheat per year (ABS, 2019). However, wheat yield varies greatly from year to year and is totally constrained by growing season rainfall. Reliable rainfall forecast across the wheatbelt is a critical first step to help growers reduce yield losses from drought. However, from our knowledge, most of previous studies were conducted in specific locations of a certain region, usually a state, and none has ever taken the Australian cropping areas as the domain. Cropping areas are critical areas that will directly benefit from reliable rainfall or drought forecasts. Furthermore, most studies focused on the prediction of next month or next 3 months and few have ever concentrated on the specific growing season (e.g. Apr.-Nov.) of the Australian cropping areas (Sacks et al., 2010). Growing season drought forecasts will provide more preparation time in comparison with seasonal forecasts for farmers to develop drought mitigation strategies. In addition, most previous studies developed linear models considering up to 9-month lead-time impacts of the climate drivers to find the predictability (Hossain et al., 2018). Given the complex effects of climate drivers on Australian rainfall, those linear models might fail to account for the climate drivers with more lead times. The dominant driver in a certain location and its nonlinear effect on rainfall also remain unknown.

Therefore, from the motivation of better understanding the relationship between growing season rainfall and various lagged large-scale climate drivers, the present study investigated growing season rainfall in the Australian wheatbelt as a case study. Instead of forecasting the absolute rainfall amount, we adopted the Standardized Precipitation Index (SPI) (Deo et al., 2017) as the dependent variable, which made the rainfall conditions comparable across different geographic regions. Moreover, it is also a commonly used meteorological drought index evaluating the degree of aridity for a certain location. We implemented a popular machine learning method, RF, as the regression technique to build forecasting models, instead of traditional linear models. The primary objectives of this study are to 1) develop growing season SPI forecasting models using various lagged large-scale climate drivers for each climate station throughout the Australian wheatbelt, 2) identify the best forecasting model for each location and compare their performance across the wheatbelt, 3) quantify the effects of the dominant climate drivers for each station on determining growing season SPI.

2. Materials and method

2.1. Study area

The study area was the Australian wheatbelt (Fig. 1). It is confined to a relatively narrow band of land to the southwest, southeast, and east of the country with a Mediterranean or temperate climate. Actual crop growing regions across the wheatbelt are about 46 million hectares, accounting for 6% of Australia's total land area (ABS, 2019). Most of Australia's agriculture, in particular its grain production, is conducted in the wheatbelt. The most important crop is winter wheat in most regions of the wheatbelt. Winter wheat is normally planted under rainfed conditions across the wheatbelt. Typical growing season of winter wheat is from April to November.

2.2. Data

2.2.1. Rainfall data

Long-term (1889 to 2018) historical daily rainfall data were obtained from Scientific Information for Land Owners (SILO) (Long Paddock, 2019), which is hosted by the Queensland Department of Environment and Science. SILO databases are constructed from observational records provided by the Australian Bureau of Meteorology. The databases consist of over 18,000 climate stations across Australia. We firstly filtered out the stations identified to be located inside the Australian wheatbelt and ultimately obtained 6726 climate stations (Fig. S1). Daily rainfall values were then simply summed up into monthly values for each station. Monthly rainfall series were then used for calculating SPI in subsequent analysis.

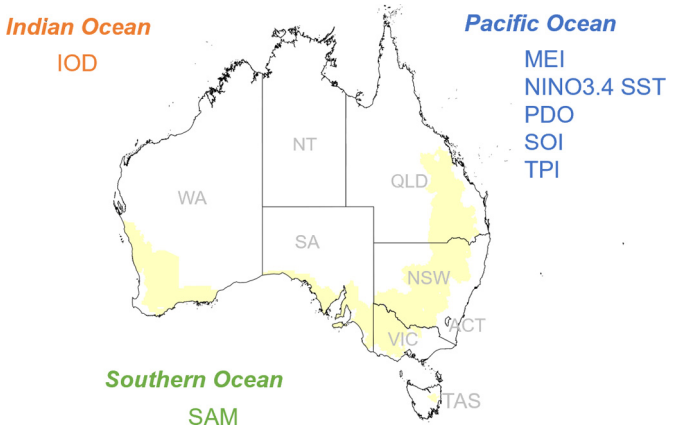

Fig. 1. The Australian wheatbelt and influential large-scale climate indices from Australia's surrounding oceans. Yellow areas inside the Australian continent denote the Australian wheatbelt. WA: Western Australia; NT: Norther Territory; QLD: Queensland; SA: South Australia; NSW: New South Wales; ACT: Australian Capital Territory; VIC: Victoria; TAS: Tasmania; IOD: Indian Ocean Dipole; SAM: Southern Annular Mode; MEI: Multivariate ENSO Index; NINO3.4 SST: NINO3.4 sea surface temperature; PDO: Pacific Decadal Oscillation; SOI: Southern Oscillation Index; TPI: the Interdecadal Pacific Oscillation Tripole Index. (For interpretation of the references to colour in this figure legend, the reader is referred to the web version of this article.)

2.2.2. Large-scale climate indices

The Australian continent is surrounded by three oceans, i.e. the Pacific, Indian, and Southern Oceans. Thus, Australia's rainfall conditions are regulated by the climatic drivers of the three oceans. These climate drivers include SST fluctuation, air pressure fluctuation, atmospheric circulation (e.g. Walker and Hadley cells), etc. In the past decades, multiple indices have been developed to describe various aspects of ocean's activities. For example, the Southern Oscillation Index (SOI) is calculated based on the surface air pressure differences between Darwin and Tahiti, which is one of the key atmospheric indices that gauge the strength of ENSO-related events in the Pacific Ocean. We selected 7 influential and commonly used large-scale climate indices as potential predictors in our study. A brief description of each selected index is given in Table 1. Monthly data from 1889 to 2018 for each index were obtained from ESRL (2019).

2.2.3. Wheat yield data

As this study attempted to forecast growing season drought conditions for cropping areas, a typical evaluation criterion was whether forecasted drought conditions could reflect crop yield for a target year. Since crops are mainly grown under rainfed conditions across the wheatbelt, crop yield is likely to be highly correlated with growing season drought conditions. Thus, we obtained region-level wheat yield observations from the Australian yield gap map (Yield Gap Australia, 2019) to evaluate the quality of forecasted drought conditions. In this map, the Australian wheatbelt is divided into 149 SA2 (Statistical Areas Level 2) regions for yield statistics (ABS, 2019). Region-level wheat yield observations for 2001–2014 are available for each region and were used in subsequent data analysis.

2.3. Standardized precipitation index

Previous studies in Australia focused on forecasting absolute rainfall amount for next few months in multiple locations of a certain small region (Hossain et al., 2019; Mekanik et al., 2016). In this condition, these locations tended to have similar annual rainfall and interannual

Table 1
Seven large-scale climate indices used in this study.

Name	Abbreviation	Description	Ocean	Key reference
Indian Ocean Dipole	IOD	A sea surface temperature dipole between the western and eastern tropical Indian Ocean	Indian	(Saji et al., 1999)
Southern Annular Mode	SAM	Pressure dipole between the Antarctic and Southern Hemisphere midlatitudes	Southern	(Thompson and Wallace, 2000)
Multivariate ENSO Index	MEI	A holistic representation of ENSO-caused atmospheric and oceanic anomalies using multiple variables	Pacific	(Wolter and Timlin, 1998)
Nino3.4 sea surface temperature	NINO3.4	Mean SST over the Nino3.4 region (5°N–5°S, 120°–170°W)	Pacific	(Kaplan et al., 1998)
Pacific Decadal Oscillation	PDO	A long-lived ENSO-like pattern of Pacific climate variability	Pacific	(Mantua and Hare, 2002)
Southern Oscillation Index	SOI	An indication of the development and intensity of El Niño or La Niña events	Pacific	(Horel and Wallace, 1981)
Tripole Index	TPI	A robust and stable representation of the Interdecadal Pacific Oscillation phenomenon	Pacific	(Henley et al., 2015)

variability. In our study, we intended to forecast rainfall conditions for a continent-wide wheatbelt. Average rainfall amount during a given period can vary significantly from location to location. Thus, to make it comparable between locations, we adopted the Standardized Precipitation Index (SPI) as the proxy to evaluate rainfall conditions in each climate station across the wheatbelt. SPI is a well-reviewed meteorological drought index and has been recommended as a key drought index by the World Meteorological Organization (Wilhite, 2006). It is a probability-based indicator that reflects the degree to which accumulated precipitation for a certain period departs from the average condition (McKee et al., 1993). It is determined by normalizing aggregated monthly precipitation based on an equi-probability transformation. In brief, aggregated monthly precipitation series (usually 1, 2, 3, …, or 24 months) is firstly fitted to a probability distribution. Then the non-exceedance probability related to such aggregated values is calculated. The corresponding standard normal quantile is defined as the SPI. In the study, we followed McKee et al. (1993) and adopted a Gamma distribution function and maximum likelihood method to calculate SPI.

The SPI is a standardized index, usually ranging from −4 to 4. A value of 0 denotes the median precipitation amount (i.e. normal condition), while positive values indicate wet conditions (i.e. >2 for extremely wet) and negative values indicate dry conditions (i.e. <−2 for extremely dry). SPI can be calculated on various timescales from 1 to 48 months to track dry and wet conditions. In this study, we calculated SPI at 8-month timescale (Apr.-Nov.) to characterize wheat growing season drought conditions.

2.4. Bias-corrected random forest

Random forest (RF) was implemented as the regression method to quantify the relationship between growing season SPI and lagged large-scale climate indices across the wheatbelt. RF is a popular tree-based ensemble machine learning algorithm and can be used to develop predictive models for both regression and classification purposes (Breiman, 2001; Chen et al., 2020; Rahmati et al., 2020). We choose random forest because its predictive performance can compete with other commonly used supervised learning algorithms, such as boosted regression trees (Park et al., 2016) or support vector machine (Naghibi et al., 2017). Moreover, RF is inherently interpretable. It can provide a reliable global variable importance estimate (Liaw and Wiener, 2002) and can also evaluate the marginal effect of a predictor variable on the response variable (Friedman, 2001).

Ensemble algorithm is a method that generates an averaged result from multiple learning models. In the case of RF, it first builds a forest of decision trees using bootstrap aggregating method (Heung et al., 2014), in which each tree is independently created based on randomized subset of predictor variables. All trees in the forest grow to maximum size without pruning and the mean of the outputs from all of the trees is determined to be the final outcome (Cutler et al., 2007). Due to the ensemble algorithm, RF is able to effectively reduce the uncertainty, leading to better performance compared to single tree-based approaches (Hastie et al., 2009).

RF predictions are averaged values of all trees' outputs. This is a valuable feature that enables RF to avoid abnormal predicted values. However, when dealing with extreme conditions, RF predictions may have biases. For example, predictions tend to be underestimated when observations are large, while overestimated when observed values are small. As our study focused on forecasting of growing season drought conditions which can be considered as extreme conditions, an effective bias correction approach was needed in order to produce reliable forecasts. In our study, an approach developed by Zhang and Lu (2012) was adopted to estimate and correct bias of the original RF model. This approach is simple and efficient and its performance with real data is satisfactory (Feng et al., 2019; Zhang and Lu, 2012). Detailed processes of this bias-correction approach are summarized below.

1) Use training dataset to fit an RF model $Y_{train} = \mathrm{RF}(X_{train})$, in which X_{train} and Y_{train} denote independent and dependent variables from the training dataset.
2) Obtain the predicted values $\hat{Y}_{train}$ from the RF model above and calculate the residuals by $r_{train} = Y_{train} - \hat{Y}_{train}$.
3) Use the training dataset as independent variables and the residuals as the dependent variable to fit an RF model $r_{train} = \mathrm{RF}_{res}(X_{train}, Y_{train})$.
4) Obtain predicted values (Y_{test}) based on the test dataset and the RF model fitted in step (1).
5) Use the RF_{res} model fitted in step (3) with independent variables in the test dataset and predicted values from step (4) to calculate the estimated residuals $r_{test} = \mathrm{RF}_{res}(X_{test}, Y_{test})$.
6) Correct bias by adding the estimated residuals to the predicted values $Y_{bias-correction} = Y_{test} + r_{test}$.

2.5. Model development and evaluation

There are 6726 climate stations across the wheatbelt, and growing season drought conditions may vary greatly among the stations. Moreover, the impacts of a certain climate driver also vary in different regions (Risbey et al., 2009). Thus, we intended to build a growing season SPI forecasting model for each station separately. As the response variable, wheat growing season SPI was derived from the monthly rainfall data of each of 6726 stations during 1889–2018. Predictor variables for all stations were large-scale climate indices prior to the growing season (Apr.-Nov.). Previous studies usually used lagged climate indices of previous 3 months to forecast rainfall in Australia (Mekanik et al., 2016). In the present study, we adopted lagged climate indices of previous 12 months ($\mathrm{Apr.}_{n-1}$-$\mathrm{Mar.}_{n}$, n is the year for which growing season SPI is forecasted), to explore whether large-scale climate drivers with longer lead time still had impacts on rainfall conditions of next year. Thus, 84 (7 indices * 12 months) predictor variables were involved in the forecasting model for each climate station.

Including 84 predictor variables in a single forecasting model might be susceptible to increased computation time and over-fitting problems because of the "curse of dimensionality" (Feng et al., 2019). Thus, identifying the most informative subset of predictor variables for each climate station was necessary. In the present study, we adopted the Boruta approach (Kursa and Rudnicki, 2010) to exclude redundant predictor variables. This approach is designed as a wrapper built around the Random Forest algorithm. It iteratively excludes the variables which are proved to be less relevant than random probes by a statistical test and capture all important predictor variables in the dataset with respect to the dependent variable. Detailed descriptions of the Boruta approach can be found in Kursa and Rudnicki (2010). We applied this approach for each climate station prior to developing the SPI forecasting model using the "Boruta" package in R software (R Core Team, 2019).

For each climate station, the dataset was randomly divided into two independent datasets, the calibration dataset (80%) and the validation dataset (20%). Then the RF model was fitted using the calibration dataset and was evaluated using the validation dataset for each station. We used default values of two parameters in the RF model, i.e. $\boldsymbol{m_{try}}$: total number of input predictors divided by 3 and $\boldsymbol{n_{tree}}$: 500. This process was executed 100 times to assess the stability of the model. The Pearson's correlation coefficient (r) and normalized Root Mean Square Error ($nRMSE$) were used for the evaluation of model performance:

$$r = \frac{\sum_{i=1}^{n}\left(O_i-\overline{O}\right)\left(P_i-\overline{P}\right)}{\sqrt{\sum_{i=1}^{n}\left(O_i-\overline{O}\right)^2}\sqrt{\sum_{i=1}^{n}\left(P_i-\overline{P}\right)^2}} \quad (1)$$

$$nRMSE = \frac{\sqrt{\frac{1}{n}\sum_{i=1}^{n}\left(P_i-O_i\right)^2}}{O_{\max}-O_{\min}} * 100\% \quad (2)$$

where n is the number of samples, O_i and P_i are observed and predicted values, $\overline{O}$ and $\overline{P}$ are the mean of observed and predicted values, $O_{\max}$ and $O_{\min}$ are maximum and minimum observed values. r measures the strength of a linear association between predicted and observed values. While $nRMSE$ represents the relative standard deviation of the residuals (prediction errors). Generally, the model performs increasingly well as r approach 1. For $nRMSE$, if it is lower than 10.0%, performance of the model is considered excellent; higher than 10.0% but lower than 20.0%, good; higher than 20.0% but lower than 30.0%, fair; higher than 30.0%, poor (Dettori et al., 2011; Nouri and Homaee, 2018). In addition, we also conducted a model test procedure by forecasting growing season SPI of several target years (2016, 2017 and 2018) using the model developed based on all available data from previous years for each target year. This procedure could help evaluate the performance of the RF model in practical drought forecasting. In this procedure, $nRMSE$ and the Q-Q (Quantile-Quantile) Plot (Tsai and Yang, 2005) between forecasted values and observed values were used to evaluate model performance. The Q-Q Plot presents a quantile-quantile plot of the quantiles of forecasted values and the quantiles of observed values. If the two kinds of values come from a same distribution, then points in the plot follow the y = x line.

3. Results

3.1. Descriptive statistics of SPI and climate indices

Long term growing season SPI was calculated for all climate stations across the wheatbelt. The distribution of SPI values from all climate stations in each year was illustrated using a box shown in Fig. 2. Red and blue shaded areas in Fig. 2 reflect dry and wet periods in the history. There was great inter-annual variability of growing season SPI in the wheatbelt. Years with serious dry conditions occurred frequently over the past hundred years, such as 1902, 1940, 1982, and 2002. Each period usually lasted for 1–8 years and then an opposite period occurred. This alternation phenomenon might relate to oscillation activities occurred in the surrounding oceans of Australia. In addition, we also noticed that the interval between 10th percentile and 90th percentile was large and stretched across the y = 0 line in most years. This meant that drought conditions could vary greatly in different climate stations in a same year given such a broad area. Thus, exploring the relationships between growing season drought conditions and oceanic oscillation activities in each climate station separately was necessary.

We then calculated Pearson's correlation coefficients at all climate stations to give a preliminary outlook of the relationships between growing season SPI and each selected climate indices. In general, MEI and NINO3.4 were positively correlated with growing season SPI, but SOI was negatively correlated with SPI (Fig. 3). While for other indices, correlation coefficients depended on lagged months. For example, TPI had negative correlations with SPI in adjacent months (Mar. and Feb.) with growing season but positive correlations with earlier months.

The italic number below each correlation coefficient value in Fig. 3 indicates the number of stations with a significant correlation. For example, there were 2611 sites where January SOI had a significant correlation with growing season SPI. NINO3.4 in antecedent May and TPI in antecedent July also significantly correlated with SPI in many stations. Large-scale climate indices of previous year might also have prospective impacts on growing season drought conditions of current year. In addition, the absolute r values were small and usually around 0, which indicated that the teleconnections between climate drivers and SPI were weak. Pearson's correlation only measures the strength of a linear

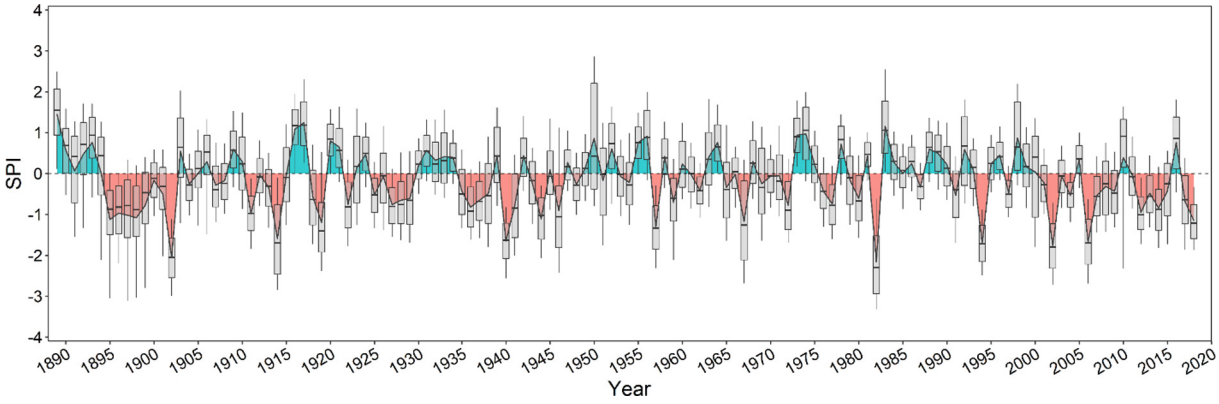

Fig. 2. Time series of centennial (1889–2018) growing season SPI for all climate stations across the wheatbelt. The box for each year reflects the distribution of SPI values from all stations. The black line within each box, two box boundaries, and whiskers below and above each box indicate median, 25th and 75th percentiles, and 10th and 90th percentiles, respectively. We linked up the mean values from all distributions using a continuous thick black line. Then, alternation of dry and wet periods during the past hundred years can be clearly illustrated based on the red and blue shaded areas under and above y = 0 line. (For interpretation of the references to colour in this figure legend, the reader is referred to the web version of this article.)

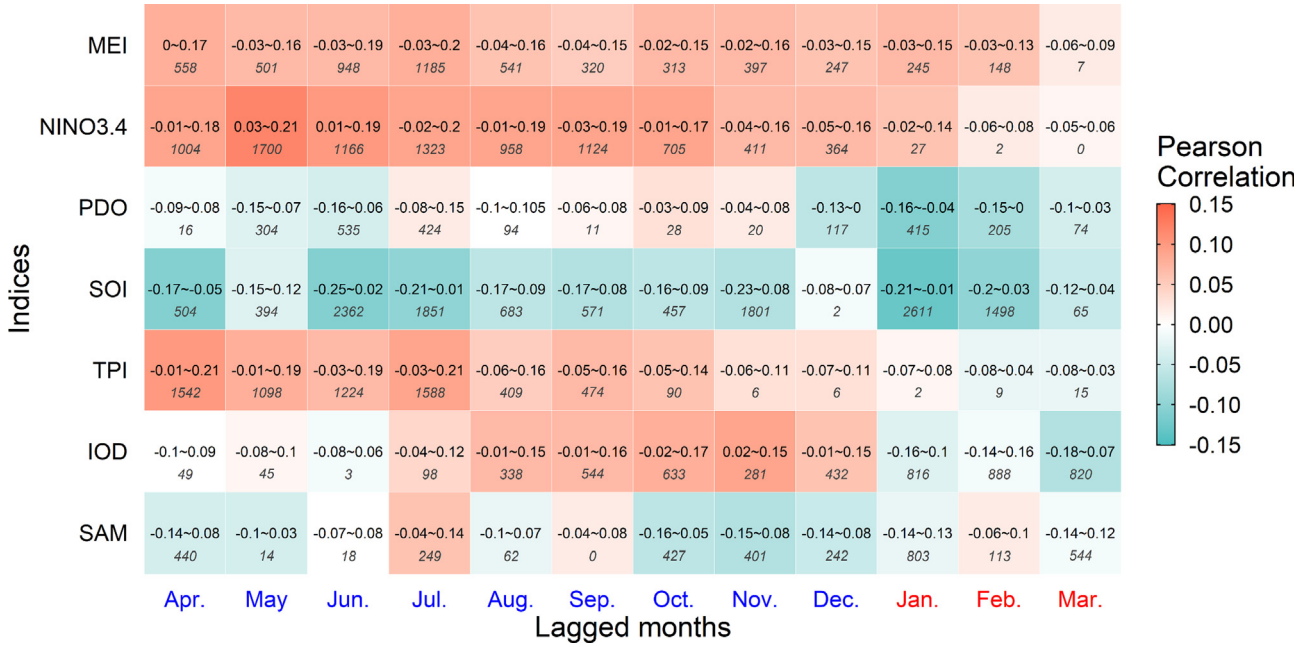

Fig. 3. Pearson's correlation coefficients between growing season SPI and lagged large-scale climate indices based on all climate stations across the Australia wheatbelt. 12-month (Jan.-Mar. in target year and Apr.-Dec. in antecedent year) values of 7 climate indices prior to the growing season were used. Mean value of correlation results of all climate stations for each index is shown as gradient colour, while 10th-90th values of correlation results are given in text. The italic number below each value indicates the number of stations showing significant correlation ($P < 0.05$). Months labels with red colour and blue colour indicate months of target year and antecedent year respectively (A same rule is also applied to other Figures and Tables). (For interpretation of the references to colour in this figure legend, the reader is referred to the web version of this article.)

association between two data series. There may be other relationships (e.g. nonlinear) that we would use the RF algorithm to explore in subsequent analysis.

3.2. Model performance

We developed drought forecasting models for each individual climate station. Mean values of two model performance metrics (*r* and *nRMSE*) from 100 runs of each station's model are shown in Fig. 4. 10th and 90th percentile values of the two metrics are present in Fig. S2 in the Supplementary material. Overall, the bias-corrected RF model performed better in the east of Australia than in the west. *r* and *nRMSE* values in the east were mostly above 0.5 and below 23% respectively, compared to 0.3 and 27% in the west. Thus, growing season drought could be better forecasted in eastern Australia using lagged climate indices. This might be due to that most climate indices used in this study were from the Pacific Ocean, but western Australia is geographically far away from the Pacific and is less affected by the Pacific (Risbey et al., 2009).

We also conducted a model validation process by forecasting growing season drought conditions of a target year using the model developed based on all available data from previous years. Observed and forecasted SPI values for three recent and representative years 2016, 2017, and 2018 are shown in Fig. 5. As 2016 was a wet year, 2017 was a near normal year, and 2018 was a dry year (Fig. 2), these forecasting results could evaluate whether the RF model could potentially provide effective drought forecasts upon years with different drought conditions. As shown in Fig. 5, RF-forecasted drought conditions were generally consistent with observed drought conditions during the wet, the normal, and dry years. Two metrics, the Q-Q Plot and *nRMSE*, were

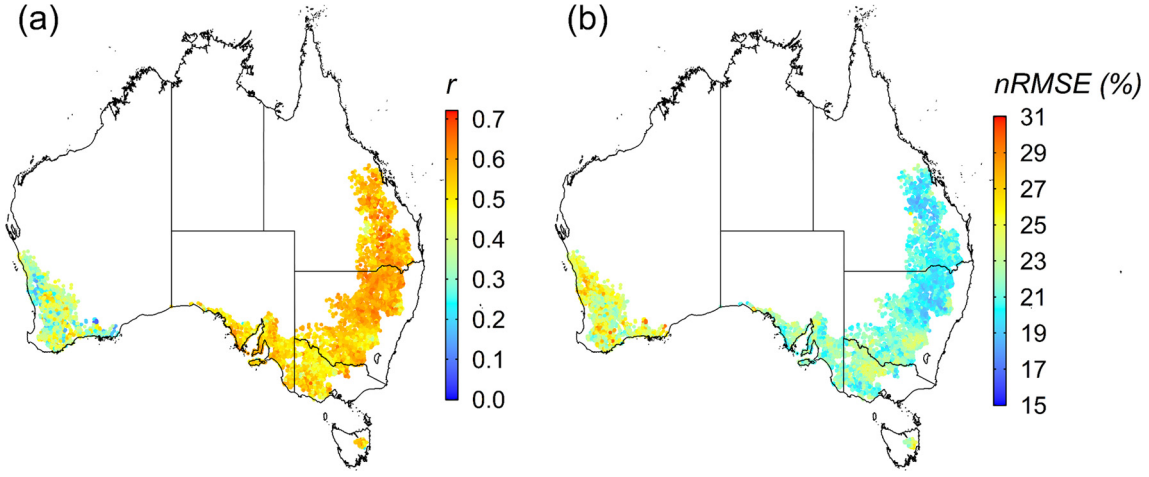

Fig. 4. Model performance metrics (Pearson's correlation coefficient (*r*) and normalized Root Mean Square Error (*nRMSE*)) for forecasts of growing season SPI using random forest (RF) models and with lagged large-scale climate indices. Results were averaged values of two statistical metrics based on 100 independent runs of model development procedure for each climate station.

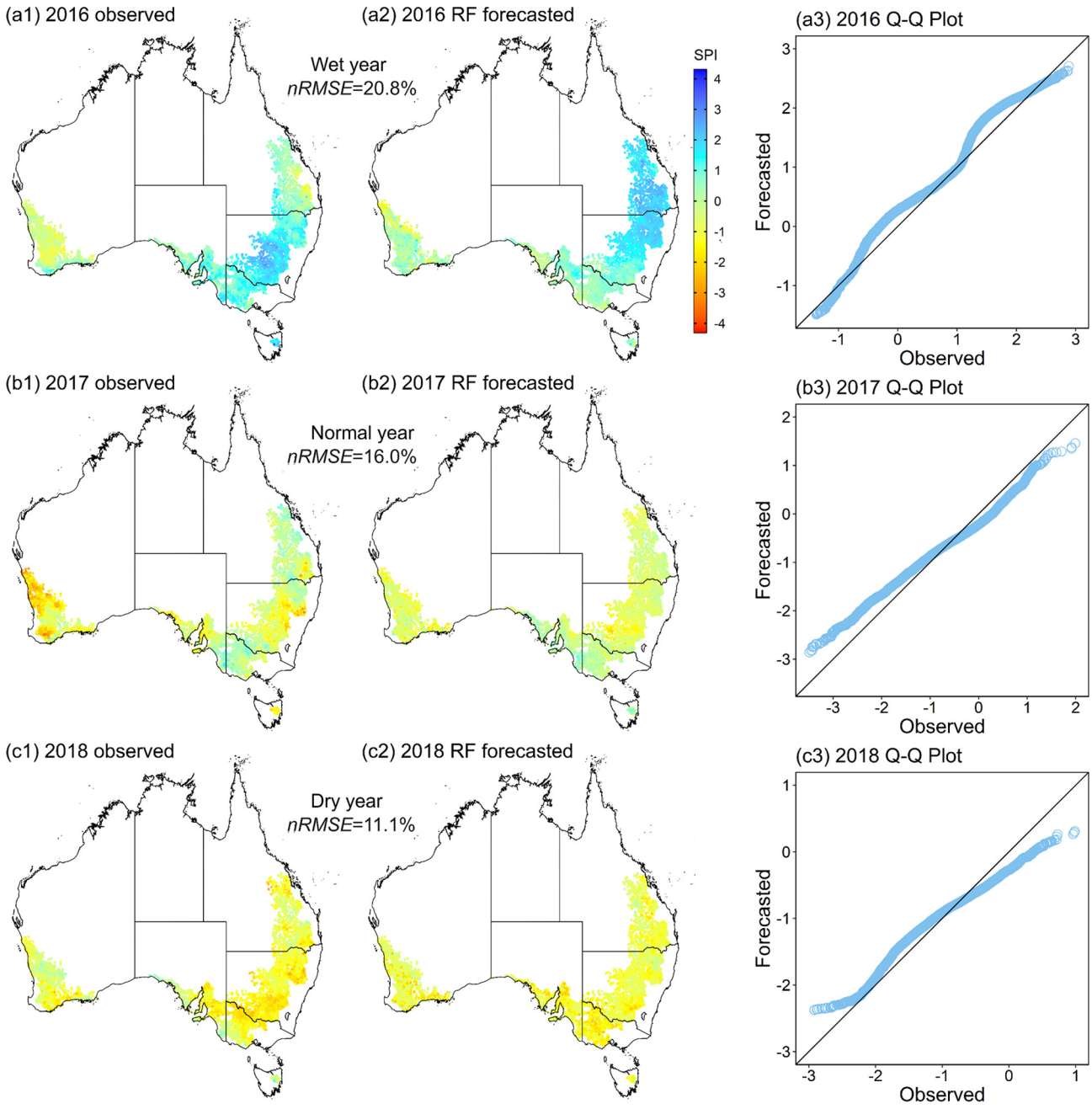

Fig. 5. Comparison between observed and RF-forecasted growing season drought conditions for three representative years, 2016, 2017, and 2018. Normalized Root Mean Square Error (*nRMSE*) and Q-Q (Quantile-Quantile) plots of observed and RF-forecasted SPI values across the Australian wheatbelt are used to evaluate model performance.

used to compare observed and forecasted drought conditions quantitatively (Fig. 5). The Q-Q Plot indicated a good match between the forecasted and observed drought conditions for each year, as points generally followed the y = x line. This meant that overall drought level was generally well captured by the RF model. Meanwhile, *nRMSE* also suggested fair predictions for each year, as *nRMSE* were all below 30%.

3.3. Dominant large-scale climate index

The RF model can provide a list of variables' importance values based on each variable's relative influence on model accuracy (Breiman, 2001). Averaged importance values for each involved climate index based on 100 runs were used to determine the dominant climate index for a certain station. Spatial distribution of these dominant climate indices is presented in Fig. 6. This figure could provide insights on the dominant climate index of different zones affecting growing season drought conditions. The lagged NINO3.4 as the most important index had broadly spread influence in nearly all zones of the wheatbelt. In particular, NINO3.4 in Oct., Dec., and Jul. of antecedent year were the dominant indices in modulating growing season drought conditions of current year in >2500 climate stations (Tables S1–3). It was interesting to find that NINO3.4 in Jan-Mar mainly affected drought conditions in eastern Australia, while NINO3.4 in antecedent year was dominant in southern and southwestern Australia. MEI, another index from the Pacific, also had dominant impacts on drought conditions in many stations. MEI in months adjacent to growing season tended to have greater effects on drought conditions compared to MEI in earlier months. By contrast, MEI in last year dominated SPI change in most southern and southwestern Australia. In addition, we also found that

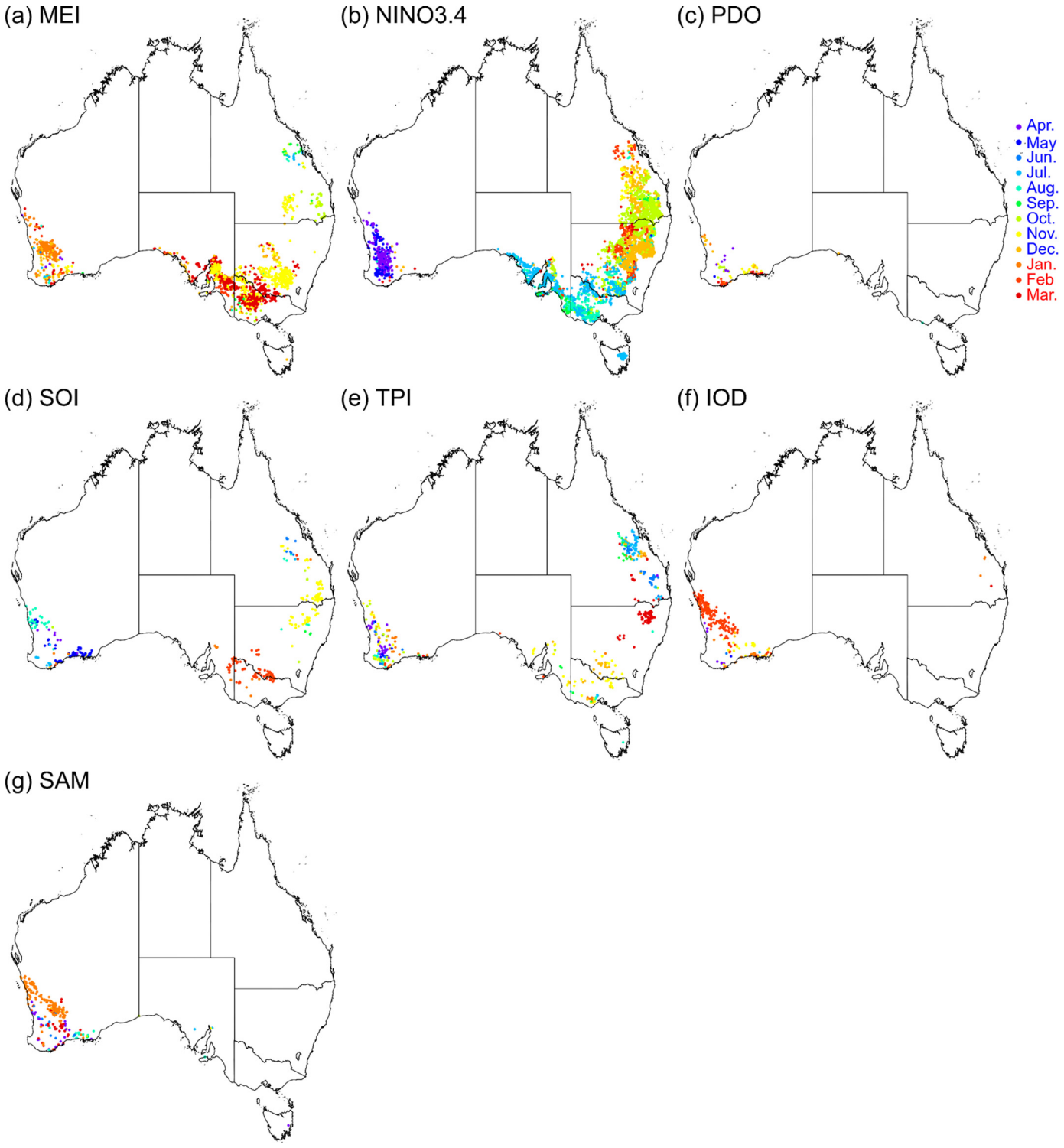

Fig. 6. Spatial distribution of locations dominated by each lagged monthly climate index. Results were obtained based on 100 independent runs of model development procedure for each station. Mean variable importance values generated from the RF model were used to determine the most important climate index for each station.

monthly IOD and SAM were recognized as the most important in many stations in southwestern Australia. This is consistent with Fig. 1, as these two climate drivers affect Australia from west to east.

As presented above, the RF model identified dominant climate index in affecting growing season drought conditions in each climate station. Investigating the dynamical responses of drought conditions to the change of dominant climate index in each station can help obtain a quick outlook of possible growing season drought conditions. Marginal effects (grey lines in Fig. 7) of dominant climate index on growing season SPI for each station were obtained from the RF model. The nature of the dependence between the response variable and the selected predictor variable could be described by the trends of the lines. In Fig. 7, we used actual values of each index instead of scaled values for a more intuitive presentation of the effects of dominant climate index on SPI. In general, growing season SPI of stations with a same dominant index showed similar patterns to the dominant index, as denoted by a similar trend of grey lines in each small plot of Fig. 7. MEI and NINO3.4 were the two most critical indices as denoted above and they followed "U"

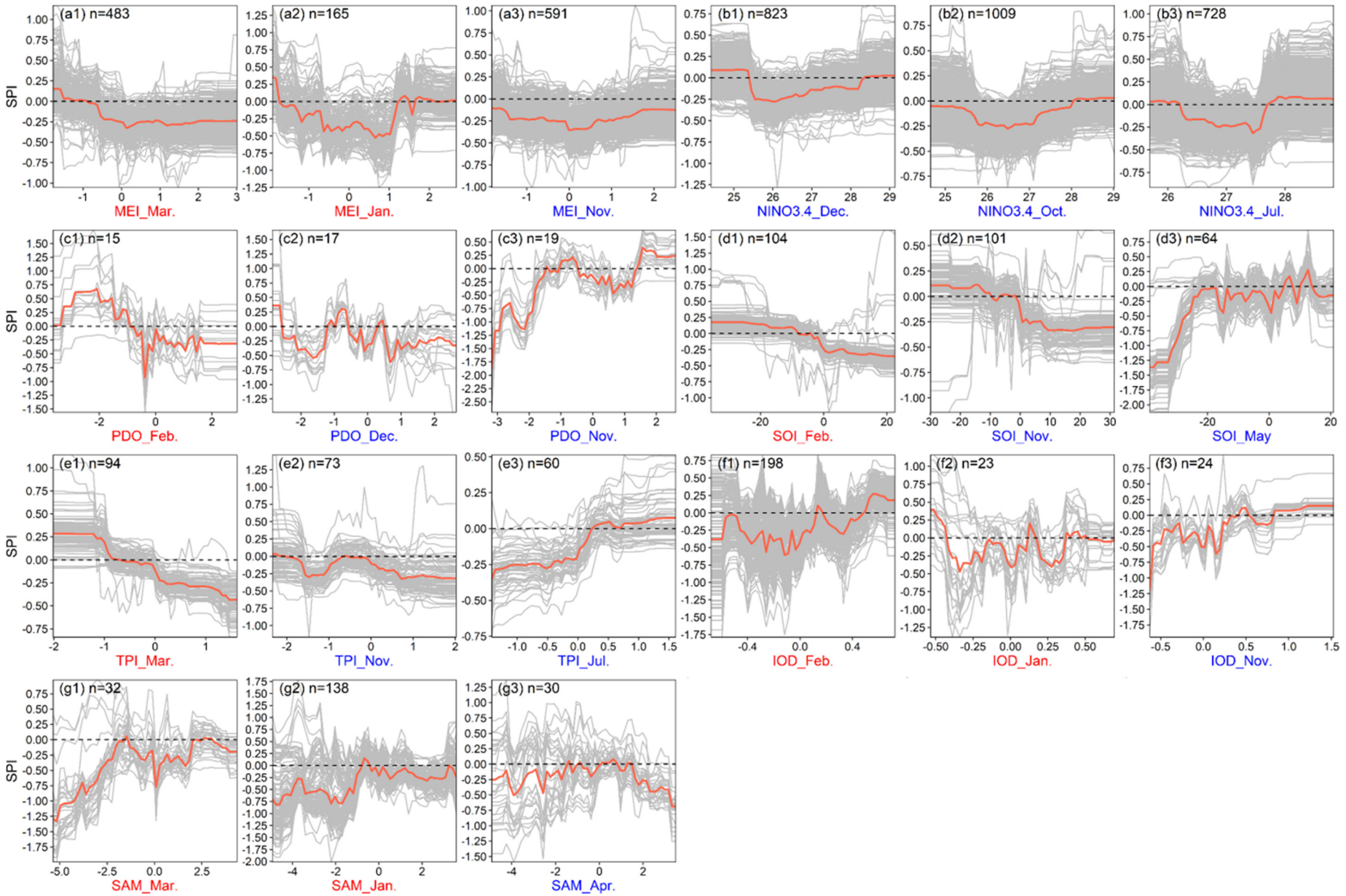

Fig. 7. Partial dependence of growing season SPI on dominant large-scale climate indices. The RF model can offer partial dependence of the change in the dependent variable for a selected predictor variable, when considering the average impact of all other predictor variables. We obtained partial dependence results of the dominant climate index (Table S1 and Fig. 6) from one run of the RF model using all available data (1889–2018) for each station. Partial dependence results of stations with a same dominant climate index were grouped. Top three months (Table S1) of each kind of climate indices are shown in each small plot above. Grey line in each small plot represents partial dependence results for all climate stations with a same dominant climate index. Red line is the averaged line based on all grey lines in each small plot. n is the number of climate stations from Table S1 for each subplot. (For interpretation of the references to colour in this figure legend, the reader is referred to the web version of this article.)

pattern relationship with growing season SPI. Drought conditions tended to occur in affected stations when MEI was around 0 and NINO3.4 was around 26–27 °C, both of which represented normal ENSO patterns. The marginal effects of other indices depended on months. For example, TPI in Mar. of current year and Nov. of antecedent year had negative impacts on SPI, while July TPI in antecedent year had positive impacts.

3.4. Correlation between forecasted SPI and crop yield

As we managed to forecast growing season drought conditions in this study, a typical evaluation criterion is whether forecasted drought conditions can reflect crop yield of target year. Thus, we calculated Pearson's correlation coefficients between forecasted SPI values and region-level wheat yield records. Before calculation, wheat yield records (2001–2014) for each region were firstly detrended using a simple and effective method, first-difference (Feng et al., 2018), to exclude yield trends caused by non-climatic factor. This method was adopted using the following equation:

$$\Delta X_n = X_n - X_{n-1}, \quad n = 2001, 2002, \ldots, 2014 \tag{3}$$

where ΔX_n denotes the first different of X at year n. Growing season SPI values for each year were forecasted by the RF model developed based on available lagged climate indices before forecasting year for each station. Then, forecasted SPI series of stations within a same SA2 region were aggregated and also detrended to calculate correlation coefficient with detrended yield series. We also calculated correlation coefficients between detrended observed SPI values and region-level wheat yield as benchmarks. As shown in Fig. 8(a), wheat yields were generally highly correlated ($r > 0.54$) with observed SPI in most regions of the wheatbelt. This means that wheat yield was largely subjected to drought conditions in the wheatbelt. Forecasted SPI showed higher correlations with wheat yields in the east of Australia than in the west. This is consistent with the results of Fig. 4, as the RF model tended to provide better drought forecasts in eastern Australia. Specifically, wheat yield in the southeast was highly correlated with forecasted SPI with correlation coefficients >0.6. However, poor correlations were also found in the northeast of the wheatbelt. This might be due to that these regions are summer dominant rainfall regions and wheat is predominantly grown on stored water from preceding summer.

4. Discussion

Australia is naturally a drought reoccurring continent. Frequent drought disasters in the past hundred years have caused great losses to agricultural production. In this study, we made use of the prognostic features of large-scale climate indices to forecast drought conditions of wheat growing season in the Australian crop belt. The results of model performance show that the bias-corrected RF model could provide acceptable drought forecasts with $r > 0.5$ and $nRMSE < 23\%$ in most parts of the wheatbelt (Fig. 4). This performance is consistent with previous studies that adopted similar data driven models as well as operational dynamical models. For example, Mekanik et al. (2016) used 3-month lagged NINO3.4, SOI, and IOD indices and adaptive network-based fuzzy inference systems models to forecast spring rainfall in 9 stations of southeast Australia. They obtained r values of 0.29–0.66 for the testing period (2000–2009), which outperformed the benchmark model method used in their study, the POAMA dynamical model. The POAMA model was previously used by Australian government to generate official weather forecasts (McIntosh et al., 2007). Although the absolute performance of the POAMA model was not excellent, it can still help stakeholders minimize losses and maximize profits in potentially "bad" seasons (Stone et al., 1996; Asseng et al., 2012a; Asseng et al., 2012b). Our proposed model focused on drought forecasts of longer lead time and showed comparable performance, thus it could provide valuable information for stakeholders across the wheatbelt to develop drought mitigation planning in advance. In addition, our research also demonstrates that using machine learning based data driven models can be a simple and effective way to provide drought outlooks in regions of interest.

The RF model in our study had better performance in the east of Australia than in the west (Fig. 4). This might be due to that we adopted more indices from the Pacific and these indices had greater prospective impacts on growing season rainfall. However, Western Australia is less affected by oceanic oscillation phenomena from the Pacific as it is geographically far away from the Pacific (Risbey et al., 2009). Meanwhile, available indices from its surrounding oceans (Fig. 1, IOD, the Indian Ocean and SAM, the Southern Ocean) might not be able to provide sufficient information for the prediction of growing season rainfall in Western Australia (Fig. 4). It is possible that there are some influential but undiscovered oceanic activities from the Indian Ocean or the Southern Ocean that affect growing season rainfall. In addition, the intensity of oceanic activities from the Indian Ocean has increased during recent decades. For example, the major driver of several main droughts in 20th century in Australia was attributed to increased occurrences of positive

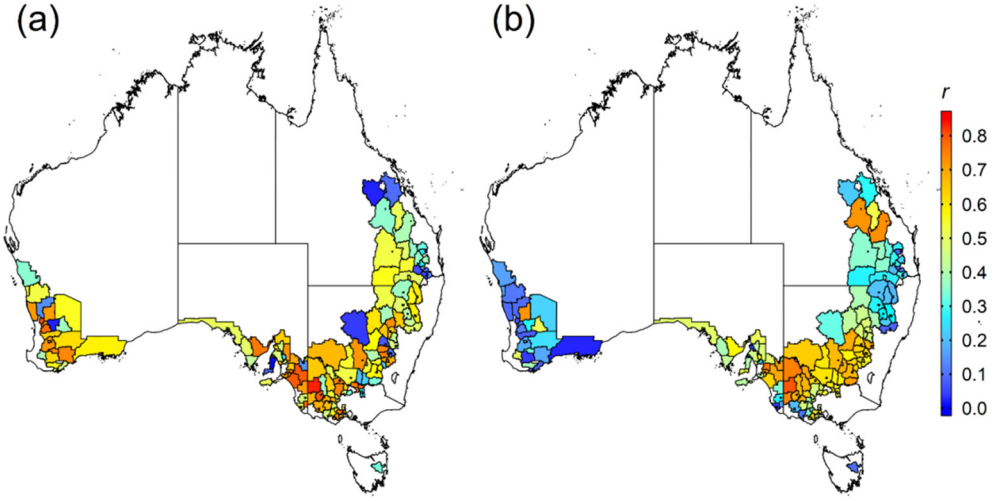

Fig. 8. Pearson's correlation coefficients between detrended wheat yield and detrended (a) observed and (b) forecasted growing season SPI for SA2 regions from 2001 to 2014. Growing season SPI was forecasted by the RF model using available lagged climate indices before a target year for each station. Observed and forecasted SPI series of stations within a same SA2 region were aggregated and then detrended to calculate correlation coefficients with detrended yield series. Values larger than 0.54 indicate significant correlations ($P < 0.05$).

IOD events rather than ENSO related phenomena (Cai et al., 2012; Nguyen-Huy et al., 2018; Yuan and Yamagata, 2015). Therefore, more efforts should be made on exploring potential oscillation activities from the Indian or Southern Oceans.

Current available large-scale climate indices have different impacts on growing season drought conditions in different zones of the wheatbelt. From the linear correlation results (Fig. 3), we found that SOI was the dominant index that affected growing season SPI. However, it was not identified as the most important index by the RF model. Instead, NINO3.4 and MEI were determined as the two most critical indices across the wheatbelt. This might be due to some nonlinear impacts from these two indices captured by the RF model. Multiple pieces of evidence have pointed out the nonlinear relationships between rainfall anomalies and ENSO events (Mekanik et al., 2013; Power et al., 2017). We also found that each index affected particular zones more than others (Fig. 6). For example, MEI, NINO3.4, SOI, and TPI from the Pacific Ocean could influence rainfall conditions of the whole wheatbelt as commonly recognized (Nicholls, 1985; Power et al., 1999). IOD and SAM mainly affected zones in Western Australia. These two climate drivers affect Australia from west to east (Fig. 1), thus they are likely to exert more impacts on rainfall conditions in western zones (Risbey et al., 2009). PDO also mainly affected zones in Western Australia, which might be because that warm PDO phases tend to coincide with anomalously wet periods in Western Australia (Mantua and Hare, 2002). In addition, some climate indices, reflecting Jul.-Dec. of antecedent year, such as MEI and NINO3.4, were identified as dominant in many climate stations (Table S1). Moreover, index of earlier months tended to affect zones that are geographically distant from the index's originating ocean. For example, NINO3.4 in previous Apr.-Jun. was the dominate index in many stations in Western Australia (Fig. 6). These results indicate that lagged impacts of oceanic oscillation activities on rainfall conditions may depend on geographical distance.

Quantifying the dynamical responses of drought conditions to the change of dominant climate index in each station can help obtain a quick outlook of possible growing season drought conditions. It is interesting to find that NINO3.4 and MEI both had nonlinear "U" pattern relationship with growing season SPI (Fig. 7). NINO3.4 indices in Dec., Oct., and Jul. of last year around 26–27 °C are likely to bring dry growing season of current year for most zones of the wheatbelt, while MEI indices around 0 tend to cause growing season drought. In addition, a certain index of different lead months might present different marginal impacts on growing season conditions. For example, SOI in last May had positive impacts, which is consistent with our current knowledge on SOI (Stone and Auliciems, 1992), while SOI in current Feb. had negative impacts (Fig. 7). Thus, actual impacts of climate indices on growing season drought conditions depend on lead months. These results can help us gain a deeper understanding of the impacts of large-scale climate indices on rainfall conditions.

Drought is commonly considered as the main factor causing yield losses in rainfed cropping region across the world (Zampieri et al., 2017). Therefore, it is necessary to test the relationship between forecasted SPI and wheat yield, which could provide valuable information for guiding agricultural practices. In this study, high correlation coefficients were found between model-forecasted SPI and observed wheat yield records in southeast of the wheatbelt (Fig. 8). As drought forecasts can be made at the end of March, farmers can have enough time to develop agronomic strategies to reduce drought-induced yield losses during crop growing season of Apr.-Nov., such as selecting appropriate cultivar or sowing date. Many previous studies have built direct relationships between preceding large-scale climate indices and yield of a certain crop (Anwar et al., 2008; Rimmington and Nicholls, 1993; Schillerberg et al., 2019) and demonstrated strong correlation between them. Our study focused on growing season drought forecasting, which could provide warning information for different kinds of crops. Nevertheless, all these studies demonstrate that use of large-scale climate indices can potentially help developing agricultural planning.

Our present study obtained comparable growing season drought forecasting results for the Australian wheatbelt based on machine learning technique and large-scale climate indices. Data of all available years were involved to develop the forecasting model. We treated each climate station independently to run the RF model for growing season drought forecast as this may provide valuable information for each individual farm in the Australian wheatbelt. Our results were obtained without considering spatial autocorrelation (Legendre, 1993). Future studies that accounts for spatial autocorrelation may help strengthen the results. Statistical models normally assume stationary relationships between the response and predictor variables. However, the impact of a given climate driver may shift over time (Ummenhofer et al., 2009). Various oceanic oscillation activities can also interact with each other and cause complex climate conditions with less predictability (Sein et al., 2015). In addition, extreme temperature can also contribute to the occurrences of drought events and is also subjected to the effects of oceanic oscillation activities in Australia (White et al., 2014). Therefore, future studies should pay more attention to non-stationary predictor-response relationships or interactions among climate drivers and use drought indices with more climate factors considered in order to obtain more reliable long-term drought forecasts.

5. Conclusions

The study developed a growing season meteorological drought forecasting model for the Australian wheatbelt using machine learning technique and multiple lagged large-scale climate indices. Observed climate data and regional wheat yield records were adopted as reference data to evaluate the performance of the drought forecasting model. Results indicate that oscillation activities from Australia's surrounding oceans could largely account for growing season drought in eastern wheatbelt. The bias corrected random forecast model was able to provide satisfactory drought forecasts in eastern parts of study area. However, the model performed poorly in the west of the wheatbelt, which highlights more research to explore oscillation phenomena occurring in the Indian or Southern Oceans.

NINO3.4 and MEI were identified as the two most critical indices that dominate growing season drought conditions across the wheatbelt. Both indices had "U" pattern relationship with growing season drought conditions. It is important to have this partial dependence plot of SPI and climate indicators because the threshold of each index could be acquired to generate immediate drought probability. In addition, we found large-scale climate drivers had lagged impacts on growing season drought conditions. Indices in previous year could also potentially affect drought conditions in current year.

Australia is a major grain producer and exporter in the world. Reliable growing season drought forecasting can effectively help stakeholders reduce drought-induced yield losses, which is of great importance for both national food supply and global food security. We believe the drought forecasting model developed in this study can provide valuable information for Australian farmers and policy makers. Moreover, the proposed forecasting model could also easily be implemented in other similar rainfed regions as input data are readily available.

CRediT authorship contribution statement

Puyu Feng: Conceptualization, Methodology, Software, Validation, Formal analysis, Writing - original draft, Visualization.**Bin Wang:**Conceptualization, Methodology, Writing - review & editing, Supervision. **Jing-Jia Luo:**Conceptualization, Writing - review & editing.**De Li Liu:** Conceptualization, Supervision, Project administration, Writing - review & editing.**Cathy Waters:**Project administration, Writing - review & editing, Funding acquisition.**Fei Ji:**Conceptualization, Writing - review & editing.**Hongyan Ruan:**Conceptualization, Writing - review & editing. **Dengpan Xiao:**Conceptualization, Writing - review & editing.**Lijie Shi:**

Conceptualization, Writing - review & editing.**Qiang Yu:**Conceptualization, Supervision, Project administration, Writing - review & editing, Funding acquisition.

Declaration of competing interest

The authors declare that they have no known competing financial interests or personal relationships that could have appeared to influence the work reported in this paper.

Acknowledgments

The first author acknowledges the China Scholarship Council (CSC) for the financial support for his Ph.D. study. Facilities for conducting this study were provided by the New South Wales Department of Primary Industries and University of Technology, Sydney. Thanks to Dr. Jian Liu of Northwest A&F University for helping re-calculating SAM.

Appendix A. Supplementary data

Supplementary data to this article can be found online at https://doi.org/10.1016/j.scitotenv.2020.138162.

References

ABARES, 2019. Australian Bureau of Agricultural and Resource Economics and Sciences, Australian Government. Available at:. http://www.agriculture.gov.au/abares/Documents/abares-insights-analysis-2018-drought.pdf, Accessed date: 14 October 2019.
Abbot, J., Marohasy, J., 2014. Input selection and optimisation for monthly rainfall forecasting in Queensland, Australia, using artificial neural networks. Atmos. Res. 138, 166–178.
ABS, 2019. Australian Bureau of Statistics, Australian Government. Available at. https://www.abs.gov.au, Accessed date: 6 June 2019.
AEGIC, 2019. Australian Export Grains Innovation Centre. Available at. https://www.aegic.org.au/, Accessed date: 14 October 2019.
Anwar, M.R., Rodriguez, D., Liu, D.L., Power, S., O'Leary, G.J., 2008. Quality and potential utility of ENSO-based forecasts of spring rainfall and wheat yield in south-eastern Australia. Aust. J. Agric. Res. 59 (2), 112–126.
Asseng, S., Thomas, D., McIntosh, P., Alves, O., Khimashia, N., 2012a. Managing mixed wheat–sheep farms with a seasonal forecast. Agric. Syst. 113, 50–56.
Asseng, S., McIntosh, P.C., Wang, G., Khimashia, N., 2012b. Optimal N fertiliser management based on a seasonal forecast. Eur. J. Agron. 38, 66–73.
Breiman, L., 2001. Random Forest. Mach. Learn. 45, 5–32.
Cai, W., Van Rensch, P., Cowan, T., Hendon, H.H., 2012. An asymmetry in the IOD and ENSO teleconnection pathway and its impact on Australian climate. J. Clim. 25 (18), 6318–6329.
Chen, W., Li, Y., Xue, W., Shahabi, H., Li, S., Hong, H., Wang, X., Bian, H., Zhang, S., Pradhan, B., Ahmad, B.B., 2020. Modeling flood susceptibility using data-driven approaches of naïve bayes tree, alternating decision tree, and random forest methods. Sci. Total Environ. 701, 134979.
Cleverly, J., et al., 2016. The importance of interacting climate modes on Australia's contribution to global carbon cycle extremes. Sci. Rep. 6, 23113.
Cutler, D.R., Edwards, T.C., Beard, K.H., Cutler, A., Hess, K.T., 2007. Random forests for classification in ecology. Ecology 88 (11), 2783–2792.
Deo, R.C., Kisi, O., Singh, V.P., 2017. Drought forecasting in eastern Australia using multivariate adaptive regression spline, least square support vector machine and M5Tree model. Atmos. Res. 184, 149–175.
Dettori, M., Cesaraccio, C., Motroni, A., Spano, D., Duce, P., 2011. Using CERES-wheat to simulate durum wheat production and phenology in southern Sardinia, Italy. Field Crop Res. 120 (1), 179–188.
Dijk, A.I., et al., 2013. The millennium drought in Southeast Australia (2001–2009): natural and human causes and implications for water resources, ecosystems, economy, and society. Water Resour. Res. 49 (2), 1040–1057.
ESRL, 2019. Earth System Research Laboratory, National Oceanic and Atmospheric Administration. Available at. https://www.esrl.noaa.gov/, Accessed date: 14 October 2019.
Feng, P., et al., 2018. Impacts of rainfall extremes on wheat yield in semi-arid cropping systems in eastern Australia. Clim. Chang. 147 (3–4), 555–569.
Feng, P., Wang, B., Li Liu, D., Yu, Q., 2019. Machine learning-based integration of remotely-sensed drought factors can improve the estimation of agricultural drought in south-eastern Australia. Agric. Syst. 173, 303–316.
Friedman, J.H., 2001. Greedy function approximation: a gradient boosting machine. Ann. Stat. 1189–1232.
Gallant, A., Kiem, A., Verdon-Kidd, D., Stone, R., Karoly, D., 2012. Understanding hydroclimate processes in the Murray-Darling Basin for natural resources management. Hydrol Earth Syst Sc 16 (7), 2049–2068.
Gergis, J., et al., 2012. On the long-term context of the 1997–2009 'Big Dry' in South-Eastern Australia: insights from a 206-year multi-proxy rainfall reconstruction. Clim. Chang. 111 (3–4), 923–944.
GLNC, 2020. Grains & Legumes Nutrition Council. Available at. https://www.glnc.org.au/grains/types-of-grains/wheat/, Accessed date: 5 March 2020.
Hastie, T., Tibshirani, R., Friedman, J., 2009. The Elements of Statistical Learning. Springer, New York. NY.
Henley, B.J., et al., 2015. A tripole index for the interdecadal pacific oscillation. Clim Dynam 45 (11—12), 3077–3090.
Heung, B., Bulmer, C.E., Schmidt, M.G., 2014. Predictive soil parent material mapping at a regional-scale: a random forest approach. Geoderma 214, 141–154.
Horel, J.D., Wallace, J.M., 1981. Planetary-scale atmospheric phenomena associated with the southern oscillation. Mon. Weather Rev. 109 (4), 813–829.
Hossain, I., Rasel, H., Imteaz, M.A., Mekanik, F., 2018. Long-term seasonal rainfall forecasting: efficiency of linear modelling technique. Environ. Earth Sci. 77 (7), 280.
Hossain, I., Rasel, H., Imteaz, M.A., Mekanik, F., 2019. Long-term seasonal rainfall forecasting using linear and non-linear modelling approaches: a case study for Western Australia. Meteorog. Atmos. Phys. 1–11.
Kaplan, A., et al., 1998. Analyses of global sea surface temperature 1856–1991. Journal of Geophysical Research: Oceans 103 (C9), 18567–18589.
King, A.D., et al., 2014. Extreme rainfall variability in Australia: patterns, drivers, and predictability. J. Clim. 27 (15), 6035–6050.
Kirono, D.G., Chiew, F.H., Kent, D.M., 2010. Identification of best predictors for forecasting seasonal rainfall and runoff in Australia. Hydrological Processes: An International Journal 24 (10), 1237–1247.
Kursa, M.B., Rudnicki, W.R., 2010. Feature selection with the Boruta package. J. Stat. Softw. 36 (11), 1–13.
Legendre, P., 1993. Spatial autocorrelation: trouble or new paradigm? Ecology 74 (6), 1659–1673.
L'Heureux, M.L., et al., 2017. Observing and predicting the 2015/16 El Niño. Bull. Am. Meteorol. Soc. 98 (7), 1363–1382.
Liaw, A., Wiener, M., 2002. Classification and regression by randomForest. R news 2 (3), 18–22.
Luo, J.-J., Liu, G., Hendon, H., Alves, O., Yamagata, T., 2017. Inter-basin sources for two-year predictability of the multi-year La Niña event in 2010–2012. Sci. Rep. 7 (1), 2276.
Mantua, N.J., Hare, S.R., 2002. The Pacific decadal oscillation. J. Oceanogr. 58 (1), 35–44.
Marshall, G.J., 2003. Trends in the southern annular mode from observations and reanalyses. J. Clim. 16 (24), 4134–4143.
McBride, J.L., Nicholls, N., 1983. Seasonal relationships between Australian rainfall and the southern oscillation. Mon. Weather Rev. 111 (10), 1998–2004.
McIntosh, P.C., Pook, M.J., Risbey, J.S., Lisson, S.N., Rebbeck, M., 2007. Seasonal climate forecasts for agriculture: towards better understanding and value. Field Crop Res. 104 (1–3), 130–138.
McKee, T.B., Doesken, N.J., Kleist, J., 1993. The relationship of drought frequency and duration to time scales. Proceedings of the 8th Conference on Applied Climatology. American Meteorological Society, Boston, MA, pp. 179–183.
Mekanik, F., Imteaz, M., Gato-Trinidad, S., Elmahdi, A., 2013. Multiple regression and artificial neural network for long-term rainfall forecasting using large scale climate modes. J. Hydrol. 503, 11–21.
Mekanik, F., Imteaz, M., Talei, A., 2016. Seasonal rainfall forecasting by adaptive network-based fuzzy inference system (ANFIS) using large scale climate signals. Clim Dynam 46 (9–10), 3097–3111.
Meneghini, B., Simmonds, I., Smith, I.N., 2007. Association between Australian rainfall and the southern annular mode. Int. J. Climatol. 27 (1), 109–121.
Mera, Y.E.Z., Vera, J.F.R., Pérez-Martín, M.Á., 2018. Linking El Niño southern oscillation for early drought detection in tropical climates: the Ecuadorian coast. Sci. Total Environ. 643, 193–207.
Naghibi, S.A., Ahmadi, K., Daneshi, A., 2017. Application of support vector machine, random forest, and genetic algorithm optimized random forest models in groundwater potential mapping. Water Resour. Manag. 31 (9), 2761–2775.
Nguyen-Huy, T., Deo, R.C., Mushtaq, S., An-Vo, D.-A., Khan, S., 2018. Modeling the joint influence of multiple synoptic-scale, climate mode indices on Australian wheat yield using a vine copula-based approach. Eur. J. Agron. 98, 65–81.
Nicholls, N., 1985. Towards the prediction of major Australian droughts. Aust. Meteorol. Mag. 33, 161–166.
Nouri, M., Homaee, M., 2018. On modeling reference crop evapotranspiration under lack of reliable data over Iran. J. Hydrol. 566, 705–718.
Paddock, Long, 2019. The Long Paddock, Queensland Government. Available at. https://www.longpaddock.qld.gov.au.
Park, S., Im, J., Jang, E., Rhee, J., 2016. Drought assessment and monitoring through blending of multi-sensor indices using machine learning approaches for different climate regions. Agric. For. Meteorol. 216, 157–169.
Power, S.B., Delage, F.P., 2018. El Niño–southern oscillation and associated climatic conditions around the world during the latter half of the twenty-first century. J. Clim. 31 (15), 6189–6207.
Power, S., Casey, T., Folland, C., Colman, A., Mehta, V., 1999. Inter-decadal modulation of the impact of ENSO on Australia. Clim Dynam 15 (5), 319–324.
Power, S.B., Delage, F.P., Chung, C.T., Ye, H., Murphy, B.F., 2017. Humans have already increased the risk of major disruptions to Pacific rainfall. Nat. Commun. 8, 14368.
R Core Team, 2019. R: A Language and Environment for Statistical Computing. R Foundation for Statistical Computing, Vienna, Austria URL. https://www.R-project.org/.
Rahmati, O., Falah, F., Dayal, K.S., Deo, R.C., Mohammadi, F., Biggs, T., Bui, D.T., 2020. Machine learning approaches for spatial modeling of agricultural droughts in the south-east region of Queensland Australia. Sci. Total Environ. 699, 134230.

Rimmington, G.M., Nicholls, N., 1993. Forecasting wheat yields in Australia with the southern oscillation index. Aust. J. Agric. Res. 44 (4), 625–632.
Risbey, J.S., Pook, M.J., McIntosh, P.C., Wheeler, M.C., Hendon, H.H., 2009. On the remote drivers of rainfall variability in Australia. Mon. Weather Rev. 137 (10), 3233–3253.
Sacks, W.J., Deryng, D., Foley, J.A., Ramankutty, N., 2010. Crop planting dates: an analysis of global patterns. Glob. Ecol. Biogeogr. 19 (5), 607–620.
Saji, N., Yamagata, T., 2003. Possible impacts of Indian Ocean dipole mode events on global climate. Clim. Res. 25 (2), 151–169.
Saji, N., Goswami, B., Vinayachandran, P., Yamagata, T., 1999. A dipole mode in the tropical Indian Ocean. Nature 401 (6751), 360.
Schillerberg, T.A., Tian, D., Miao, R., 2019. Spatiotemporal patterns of maize and winter wheat yields in the United States: predictability and impact from climate oscillations. Agric. For. Meteorol. 275, 208–222.
Sein, Z.M.M., Ogwang, B.A., Ongoma, V., Ogou, F.K., Batebana, K., 2015. Inter-annual variability of summer monsoon rainfall over Myanmar in relation to IOD and ENSO. J. Environ. Agric. Sci. 4, 28–36.
Steptoe, H., Jones, S., Fox, H., 2018. Correlations between extreme atmospheric hazards and global teleconnections: implications for multihazard resilience. Rev. Geophys. 56 (1), 50–78.
Stone, R., Auliciems, A., 1992. SOI phase relationships with rainfall in eastern Australia. Int. J. Climatol. 12 (6), 625–636.
Stone, R.C., Hammer, G.L., Marcussen, T., 1996. Prediction of global rainfall probabilities using phases of the southern oscillation index. Nature 384 (6606), 252.
Thompson, D.W., Wallace, J.M., 2000. Annular modes in the extratropical circulation. Part I: month-to-month variability. J. Clim. 13 (5), 1000–1016.
Tsai, D.M., Yang, C.H., 2005. A quantile–quantile plot based pattern matching for defect detection. Pattern Recogn. Lett. 26 (13), 1948–1962.
Ummenhofer, C.C., et al., 2009. What causes southeast Australia's worst droughts? Geophys. Res. Lett. 36 (4), 1–5.
van Rensch, P., Cai, W., 2014. Indo-Pacific–induced wave trains during austral autumn and their effect on Australian rainfall. J. Clim. 27 (9), 3208–3221.
White, C.J., Hudson, D., Alves, O., 2014. ENSO, the IOD and the intraseasonal prediction of heat extremes across Australia using POAMA-2. Clim. Dyn. 43 (7–8), 1791–1810.
Wilhite, D.A., 2006. Drought Monitoring and Early Warning: Concepts, Progress and Future Challenges. World Meteorological Organization. WMO, p. 1006.
Williams, A.A., Stone, R.C., 2009. An assessment of relationships between the Australian subtropical ridge, rainfall variability, and high-latitude circulation patterns. Int. J. Climatol. 29 (5), 691–709.
Wolter, K., Timlin, M.S., 1998. Measuring the strength of ENSO events: how does 1997/98 rank? Weather 53 (9), 315–324.
Xie, Z., et al., 2019. Multi-climate mode interactions drive hydrological and vegetation responses to hydroclimatic extremes in Australia. Remote Sens. Environ. 231, 111270.
Yield Gap Australia, 2019. Yield Gap Australia, Commonwealth Scientific and Industrial Research Organisation and Grains Research and Development Corporation. Available at. http://yieldgapaustralia.com.au/, Accessed date: 14 October 2019.
Yu, L., Gao, X., Zhao, X., 2020. Global synthesis of the impact of droughts on crops' water-use efficiency (WUE): towards both high WUE and productivity. Agric. Syst. 177, 102723.
Yuan, C., Yamagata, T., 2015. Impacts of IOD, ENSO and ENSO Modoki on the Australian winter wheat yields in recent decades. Sci. Rep. 5, 17252.
Zampieri, M., Ceglar, A., Dentener, F., Toreti, A., 2017. Wheat yield loss attributable to heat waves, drought and water excess at the global, national and subnational scales. Environ. Res. Lett. 12 (6), 064008.
Zarch, M.A.A., Sivakumar, B., Sharma, A., 2015. Droughts in a warming climate: a global assessment of standardized precipitation index (SPI) and reconnaissance drought index (RDI). J. Hydrol. 526, 183–195.
Zhang, G., Lu, Y., 2012. Bias-corrected random forests in regression. J. Appl. Stat. 39 (1), 151–160.
Zhang, R., Chen, Z.Y., Xu, L.J., Ou, C.Q., 2019. Meteorological drought forecasting based on a statistical model with machine learning techniques in Shaanxi province, China. Sci. Total Environ. 665, 338–346.